Proceedings of ALGORITMY 2012
pp. 179–189

# COMPARISON OF THREE DIFFERENT OBSTACLE MODELS FOR MODELING OF STRATIFIED FLOWS OVER THE BODY *

LUDĚK BENEŠ † AND PHILIPPE FRAUNIÉ ‡

**Abstract.** The article deals with the numerical simulation of the stratified incompressible flows over the body. The mathematical model is based on the Boussinesq approximation of the Navier–Stokes equations for viscous incompressible stratified flow. Three different numerical approaches to the body are implemented and tested. The first one is the classical body fitted mesh. The second one is the penalization technique. The obstacle is modeled as the permeable obstacle with high resistance parameter. The last approach is based on the immersed boundary method. The resulting set of PDE's is then solved by the AUSM MUSCLE scheme in finite volume approximation. For the time integration the three stage BDF method of the second order is used.

**Key words.** Stratified flow, internal waves, obstacle modeling, penalization, immersed boundary

**AMS subject classifications.** 76D50, 76D33, 65M08

**1. Introduction.** Interest in the study of the flow structure in stratified fluid is stimulated by a number of environmental and technical problems. Stratified flows in environmental applications are characterized by the variation of fluid density in the vertical direction that can lead to appearance of specific phenomena which are not present when density is constant, namely internal and gravity waves, jet–like flow structures, thin interfaces with high density and velocity gradients and anisotropic turbulence. Even if the density changes are small, density gradients can be large. In a stably stratified fluid a buoyancy force causes very distinct flow behavior manifested by a presence of large–scale wave patterns in the flow–field. The stratification also strongly affects flow separation and downstream wake structure.

The internal waves are generated by many different processes, for example disturbances induced by moving obstacles [3], [2], [19], during the collapse of mixed regions in the stratified fluid [1], by flow past topography [4] (Lee waves) and due to perturbations induced by contiguous turbulent regions [5]. The transport of momentum and energy by these waves contributes significantly to the general dynamics of the atmosphere and study of its generation and behavior is essential for understanding of the ocean and atmosphere behavior.

The experimental and numerical studies of the flow around a moving obstacle were proposed by e.g. [2],[7],[21],[8],[16],[9].

From the numerical point of view, the simulations of stratified fluid flows are in general more demanding than the solution of similar non-stratified flow cases. The transport equation for the density (or its perturbation) is coupled to momentum equations by a buoyancy term. Because of this buoyant force the obstacles in flow generate waves that propagate at long distances. These waves need to be properly resolved, without unphysical damping or dispersion.

*This work was supported by Grant TA 01020428, GIRAC project, FUI pôle Mer, Region PACA and CG83

†Dept. of Technical Mathematics, Faculty of Mechanical Engineering, Czech Technical University in Prague (benes@marian.fsik.cvut.cz).

‡MIO, Université du Sud Toulon-Var, AMU, CNRS, IRD, France(Philippe.Fraunie@lseet.univ-tln.fr)

Our study of the stratified flow started in 2008 by the simulation of the flow past a ball in 2D [14] using WENO, AUSM MUSCL and compact differences schemes . The extension to 3D was published in [12], [13]. Next studies were devoted to the flow around thin vertical strip [15] and over sinusoidal hill [10].

The correct resolution of the flow structure over the body can be affected by its representation. Suitability of different body's models can also depend on the effects under investigation. It means whether we are interested more in the boundary layer in the proximity of the body surface or rather in the development of internal waves farther from the body. Different methods of body's modeling are studied.

**2. Boussinesq approximation.** The flow is assumed to be incompressible, yet the density is not constant. The mathematical model is based on the Navier-Stokes equations for viscous incompressible flow with variable density.

These equations are simplified by the Boussinesq approximation. Density and pressure are divided into two parts: a background field (with subscript $_0$) plus a perturbation. The system of equations obtained is partly linearized around the average state $\rho_*$. The full development of the basic system of equations can be found in [10]. The resulting set of equations for 2D flow can be written in the form

$$\frac{\partial \varrho}{\partial t} + \frac{\partial(\varrho u_j)}{\partial x_j} = -u_2 \frac{\partial \varrho_0}{\partial x_2}, \tag{2.1}$$

$$\frac{\partial u_i}{\partial t} + \frac{\partial(u_j u_i)}{\partial x_j} + \frac{1}{\varrho_*}\frac{\partial p}{\partial x_i} = \nu \frac{\partial^2 u_i}{\partial x_j \, \partial x_j} - \delta_{i,2}\frac{\varrho}{\varrho_*} g, \tag{2.2}$$

$$\frac{\partial u_j}{\partial x_j} = 0, \tag{2.3}$$

or, in vector form

$$\tilde{P}\frac{\partial W}{\partial t} + \frac{\partial F^i(W)}{\partial x_1} + \frac{\partial G^i(W)}{\partial x_2} = \nu\left(\frac{\partial F^v(W)}{\partial x_1} + \frac{\partial G^v(W)}{\partial x_2}\right) + S(W). \tag{2.4}$$

$$F^i = [\rho u_1, u_1^2 + \frac{p}{\varrho_*}, u_1 u_2, u_1]^T,\; G^i = [\rho u_2, u_1 u_2, u_2^2 + \frac{p}{\varrho_*}, u_2]^T,$$

$$F^v = [0, \frac{\partial u_1}{\partial x_1}, \frac{\partial u_2}{\partial x_1}, 0]^T, \quad G^v = [0, \frac{\partial u_1}{\partial x_2}, \frac{\partial u_2}{\partial x_2}, 0]^T, \quad S = [-u_2\frac{\partial \rho_0}{\partial x_2}, 0, -\frac{\varrho}{\varrho_*} g, 0]^T$$

where $W = [\varrho, u_1, u_2, p]^T$ is the vector of unknowns, $\varrho(x_1, x_2, t)$ denotes the perturbation of the density and $u_1$, $u_2$ are two velocity components, $p$ stands for the pressure perturbation and $g$ for the gravity acceleration and $\tilde{P} = diag(1,1,1,0)$. The $x_1$–axis is orientated in the direction of the motion and the $x_2$–axis is perpendicular to the density gradient.

The other parameters of the flow are related to the velocity of incoming flow $U$ and to characteristic height of the obstacle $h$. For the description of the stratified flow around the horizontal strip the Reynolds number, the Richardson number and the Froude number are defined as

$$Re = \frac{Uh}{\nu}, \qquad Ri = -\frac{g}{\varrho_0}\frac{\frac{\partial \varrho_0}{\partial x_2}}{U} \qquad Fr = \frac{(U)^2}{N^2 h^2},$$

the buoyancy frequency $N = \sqrt{-\frac{g}{\varrho_0}\frac{\partial \varrho_0}{\partial x_2}} = 2\pi/T_b = \sqrt{\frac{g}{\Lambda}}$, where $T_b$ is the buoyancy period, and $\Lambda = -1/\frac{\partial \ln \varrho}{\partial x_2}$ is the length scale of stratification.

**3. Numerical scheme.** For the numerical solution of the above mentioned equations the AUSM MUSCL scheme in the finite volume formulation combined with the artificial compressibility method in dual time is used.
The continuity equation (2.3) is rewritten in the form

$$\frac{\partial p}{\partial \tau} + \beta^2 \frac{\partial u_j}{\partial x_j} = 0, \tag{3.1}$$

where $\tau$ is the artificial time. The finite volume AUSM scheme is used for the spatial semidiscretization of the inviscid fluxes.

$$\int_\Omega \left(\frac{\partial F^i}{\partial x_1} + \frac{\partial G^i}{\partial x_2}\right) dS \approx \sum_{k=1}^{4} \left[ u_n \begin{pmatrix} \varrho \\ u_1 \\ u_2 \\ \beta^2 \end{pmatrix}_{L/R} + p \begin{pmatrix} 0 \\ n_x \\ n_y \\ 0 \end{pmatrix} \right] \Delta l_k, \tag{3.2}$$

where $u_n$ is the normal velocity vector, and $(q)_{L/R}$ are quantities on the left/right hand side of the face. These quantities are computed using MUSCL reconstruction with the Hemker-Koren limiter [20]

$$q_R = q_{i+1} - \frac{1}{2}\delta_R \quad q_L = q_i + \frac{1}{2}\delta_L,$$

$$\delta_{L/R} = \frac{a_{L/R}(b_{L/R}^2 + 2) + b_{L/R}(2a_{L/R}^2 + 1)}{2a_{L/R}^2 + 2b_{L/R}^2 - a_{L/R}b_{L/R} + 3},$$

$$a_R = q_{i+2} - q_{i+1} \quad a_L = q_{i+1} - q_i \quad b_R = q_{i+1} - q_i \quad b_L = q_i - q_{i-1}.$$

The scheme is stabilized according to [11] by the pressure diffusion.

$$\left(0, 0, 0, \eta \frac{p_{i+1,j} - p_{i,j}}{\beta_x}\right)^T \qquad \beta_x = w_r + \frac{2\nu}{\Delta x}$$

where $w_r$ is reference velocity (in our case the maximum velocity in flow field) and $\eta$ is the scaling factor (in our computations $\eta \in < 0, 10^{-3} >$.

The viscous fluxes are discretized using central approach on a dual mesh (diamond type scheme).

The spatial discretization results in a system of ODE's solved by the second-order BDF formula

$$\frac{3W^{n+1} - 4W^n + W^{n-1}}{2\Delta t} + L^{n+1} = 0. \tag{3.3}$$

Here, $L^{n+1}$ denotes the numerical approximation of the convective and viscous fluxes described above and the source terms. Arising set of nonlinear equations is then solved by the artificial compressibility method in the dual time $\tau$ by the explicit 3-stage second-order Runge-Kutta method.

Presented scheme was successfully validated in our previous studies. The scheme has been successfully used for simulation of the flow field around moving bodies in 2D and 3D stratified fluid and also for simulation of the flow over the hill for wide range of Richardson numbers, see [12], [13], [14], [15], [10].

**4. Obstacle modeling.** We are interested in the simulation of the flow past a body. For the obstacle modeling three different techniques have been used.

• In the first case the classical body fitted mesh surrounding the obstacle is used. Multidomain arrangement with 4 subdomains is used. Due to simplicity of our obstacle, very simple Cartesian grids can be used. In the case of the general body, the deformation of the mesh will play significant role in the numerical simulations.

• In the second case, the obstacle is modeled as a source term emulating a porous media with small permeability by the volume penalization technique proposed originally by Arquis and Caltagirone [22]. A term proportional to the difference between the fluid and obstacle velocities is added to the momentum equation and represents the drag force.

$$\frac{\chi(x,y,t)}{K_{rez}}(U_i^{ob} - u_i), \tag{4.1}$$

where $K_{rez}$ corresponds to the small permeability of the obstacle, moving with velocity $U^{ob}$. In the computed case, the obstacle is at rest and drag is proportional to the velocity of the incoming flow. $\chi(x,y,t)$ is the characteristic function of the obstacle and is equal to 1 inside the obstacle and 0 elsewhere. According to our previous numerical tests, which studied the dependence of the solution on the permeability parameter, its value is set to $K_{rez} = 1/1000$, see [12].

• Last model is based on simple variant of the immersed boundary method [18], [17]. In this modification the computational cells lying inside the body are identified. Then, the velocity in these cells is set to $U^{ob}$, while pressure and density are computed for whole domain. Similar technique was successfully used for simulation of the flow around the preservative ramparts in the open coal mine [23].

The immersed boundary approximation may seems as limiting case of the porous media for $K_{rez} \to \infty$. But these approaches represent different concepts. In the first case expected value of the velocity is prescribed directly to the flow field. In the second case the penalization term is added to the momentum equations and flow field is driven by this force.

Advantage of the last two approaches lies in a very simple computational mesh. On the other hand the question arise regarding the correct resolution of the boundary layer on the body.

**5. Computational setup.** The problem solved in this study is inspired by the towing tank measurement performed by Chaschechkin and Mitkin [16]. The thin horizontal strip $0.025 \times 0.002\ m$ is placed in the towing tank with dimensions $2.2 \times 0.6\ m$. The strip is located $1m$ from the left wall and at the mid–heights. At the time $t = 0$ the obstacle starts moving to the right (in the positive $x_1$ direction) with constant velocity $U^{ob} = 0.0017\ m/s$. The flow field is initially at rest with the exponential profile of stratification $\varrho_0 = \varrho_{00} \exp \frac{x_2}{\Lambda}$, $\varrho_{00} = 1008.9\ kg/m^3$, $\Lambda = 47.735\ m$, the kinematic viscosity is $\nu = 10^{-6} m^2/s$. It corresponds to the $Re = 3.4$ (relative to the thickness of the body) and $Ri = 121$. In our computations the body is fixed in the incoming flow of the corresponding velocity and stratification given by the experiment.

The computational domain is $0.5 \times 0.25m$. The obstacle is placed $0.3m$ from the left side (ranges in $< 0.3; 0.325 > m$) and in the middle height. The origin is placed on the left side of the domain and in the middle height. The $x_1$ axis is orientated in the stream-wise direction.

The same set of the boundary conditions is satisfied in the physical and artificial time. On the inlet, the velocity is prescribed. Pressure and density disturbances are extrapolated from the flow field. On the outlet velocity and density perturbance are extrapolated. Pressure perturbance is set to zero. On the top and bottom, homogeneous Neumann boundary conditions are satisfied. Pressure is fixed in one point. In the multidomain case, the non–slip boundary conditions are prescribed for velocity component on the body. For the pressure and density perturbations the homogeneous Neumann condition are used.

The computations have been performed on the Cartesian mesh of $500 \times 500$ cells. The resolution of the mesh is $1mm$ in the $x_1$ direction and $0.5mm$ in the $x_2$ direction. To verify independence of the solution on the mesh, and sensitivity of different approaches the mesh two times refined (resolution $0.25mm$) and two times diluted (resolution $1mm$) in $x_2$ direction was used.

**6. Numerical results.** Fig.6.1 shows the process of the wave generation in the form of isolines of $u_2$ velocity component for three different times. The multidomain approach is used. The flow pattern is typical for transient internal waves past an impulsively started body in stably stratified flow. The thin strip generates an initial perturbation and then gravity waves are formed. The upstream disturbances are pronounced, which is typical for the flow with relatively low Froude number. Behind the obstacle strip with step–like density profile is formed as is shown on Fig. 6.2 left.

In Fig.6.2, the comparison of the different obstacle approaches in the form of the isolines of density perturbance $\varrho$ (left) and $u_2$–velocity component (right) is given. The comparison shows a very good qualitative agreement. Small differences are in the wake behind the obstacle, which is stronger in the multidomain case. Immersed boundary case and permeable obstacle are practically the same.

Figs.6.3–6.4 displays the perpendicular distribution of the computed quantities in different distances. Point $x = 0.24m$ is in front of the obstacle, $x = 0.305m$ and $x = 0.315m$ are on the obstacle, $x = 0.33m$ and $x = 0.35m$ are behind the obstacle. The wave length is the same in all models and is in a good agreement with theoretical prediction given by the Brunt-Väisälä frequency. Maxima and minima of all computed quantities are the highest in the multidomain approach mainly in front of and behind the obstacle. Results in the porous and immersed boundary cases are very similar. The boundary layer on the obstacle is well resolved in all approaches, see Fig.6.4b. Main differences are in the $u_2$–velocity component. Over the centre of the strip the minimum of this component is predicted by the porous approach Fig.6.5.

Fig.6.6 shows dependency of the $u_1$ and $u_2$–velocity components on the beginning of the obstacle on the mesh for porous and immersed boundary approach. The $u_1$ component is captured relatively well on coarsest grid (the obstacle is very thin, so the mesh is not so bad), $u_2$ velocity component seems much more sensitive. On the coarsest mesh is resolved with the error greater then 20%.

The maxima of the quantities in whole computational domain are sumarized in the Tab.1. These maxima are compared to the multidomain approach and are approximately 8% lower in the immersed boundary and porous case.

**7. Conclusion.** The flow around obstacle in the stratified flow was simulated. Three different models of obstacle were implemented and compared.

Presented first results show that all models are suitable for modeling of this type of problems. Both wave structure far away the obstacle and boundary layer are well resolved. The number, position and wave length are practically identical and are

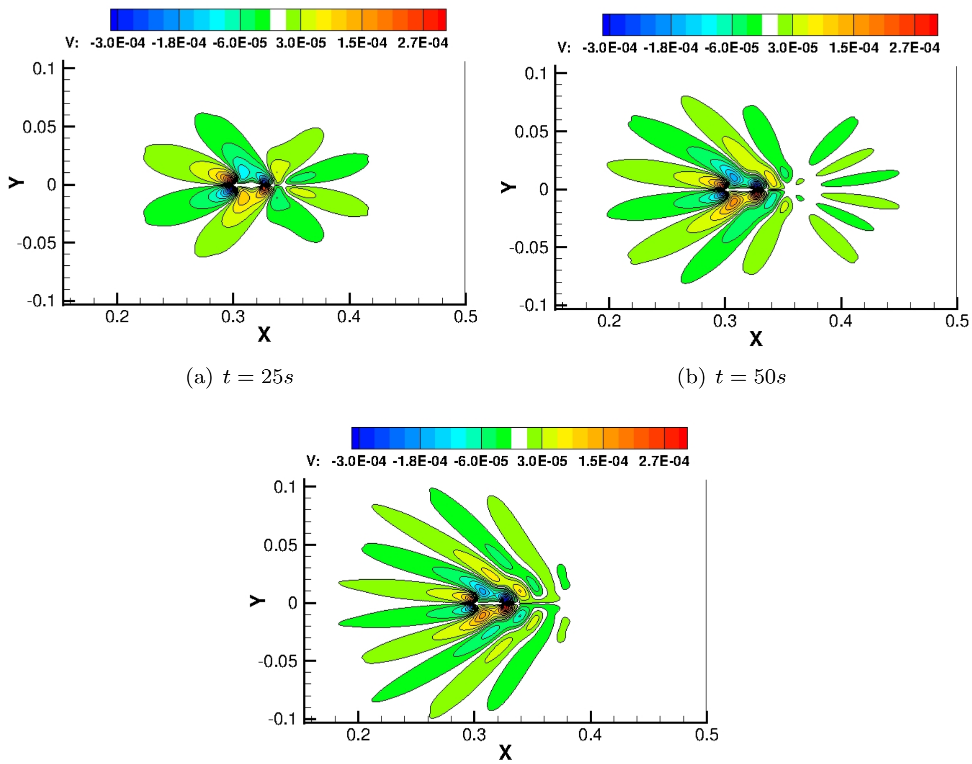


(a) $t = 25s$ (b) $t = 50s$

(c) $t = 75s$

FIG. 6.1. *Developing of the internal waves. Isolines of $u_2$– velocity component, three different times.*

| variable | multidomain | porous | immersed boundary |
|---|---|---|---|
| $\varrho$ | $4.34 \times 10^{-2}$ | $4.02 \times 10^{-2}$ | $4.04 \times 10^{-2}$ |
| difference | 0% | 7.3% | 6.9% |
| $u_1$ | $2.13 \times 10^{-3}$ | $2.11 \times 10^{-3}$ | $2.11 \times 10^{-3}$ |
| difference | 0% | 0.9% | .9% |
| $u_2$ | $3.23 \times 10^{-4}$ | $2.95 \times 10^{-4}$ | $2.97 \times 10^{-4}$ |
| difference | 0% | 8.7% | 8.0% |

TABLE 6.1

*Maxima of the computed quantities and relative differences to the multidomain case.*

in the good agreement with the theoretical prediction. The small differences are in the predicted maxima and minima of the computed quantities, which are app. 8% higher in the multidomain approach. While the $u_1$–velocity component is similar in all models (including the boundary layer), greatest differences are in the prediction of the $u_2$–velocity component. For the deeper understanding of the behavior of these models (e.g. dependency on the mesh density) further research is necessary.

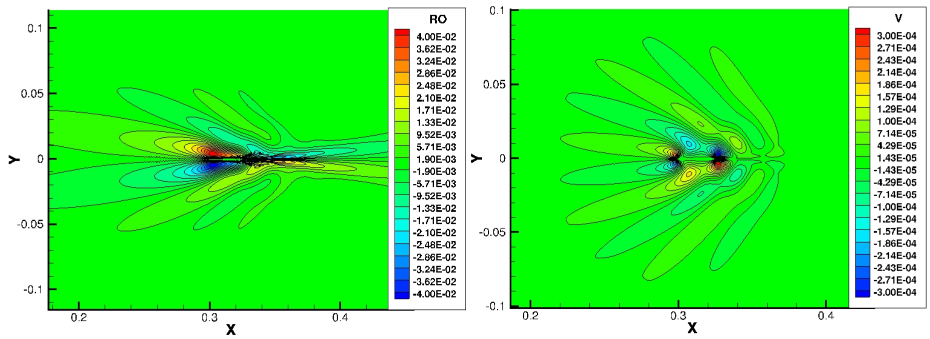


(a) multidomain – body fitted mesh

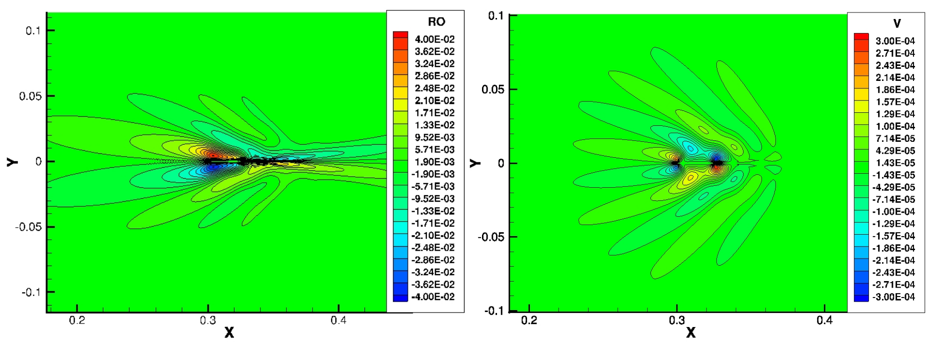


(b) permeable obstacle

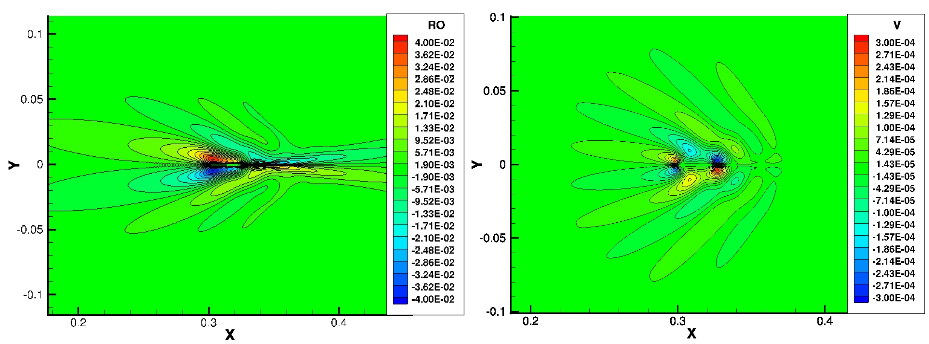


(c) immersed boundary

FIG. 6.2. *Comparison of the flow pattern at time $t = 75s$. Left column shows isolines of the density perturbance $\varrho$, right column isolines of $u_2$ velocity component.*

REFERENCES


[1] DeSilva I.P.D: Fernando HJS.: Experiment on collapsing patches in stratified fluids. *J. Fluid Mech.* **358**, 29–60, 1998

[2] Boyer D., Davies P., Fernando H., Zhang X.: Linearly stratified flow past a horizontal circular cylinder. *Phil. Trans. R. Soc. Lond.* **A328**, 501-528, 1989.

[3] Chashechkin Y., Gumennik E., Sysoeva E.: Transformation of a density field by a three-dimensional body moving in a continuously stratified fluid. *J. Appl. Mech. Tech. Phys.* **36(1)**, 19-29, 1995.

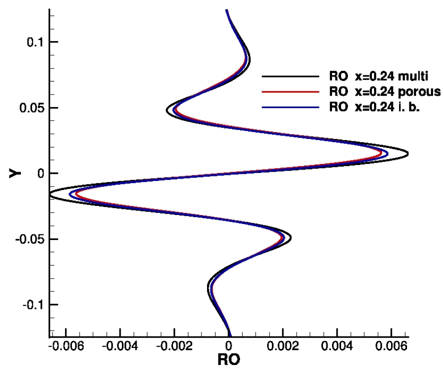


(a) $x = 0.24m$

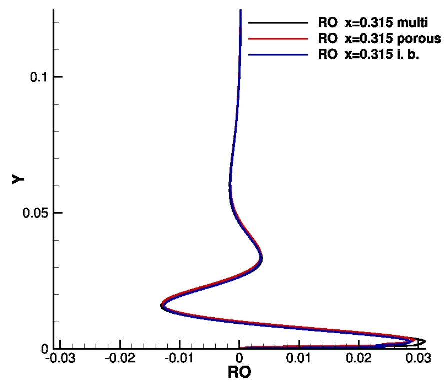


(b) $x = 0.315m$

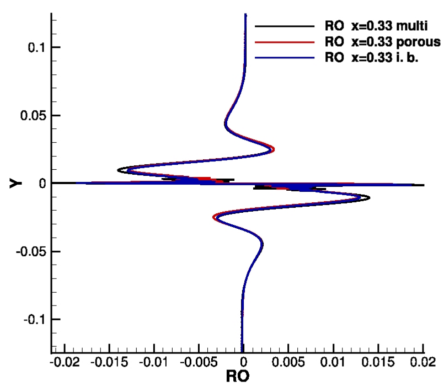


(c) $x = 0.33m$

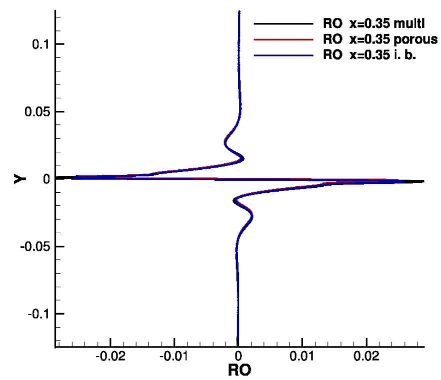


(d) $x = 0.35m$

FIG. 6.3. *Vertical profiles of the density perturbation $\varrho$ in the different distances.*

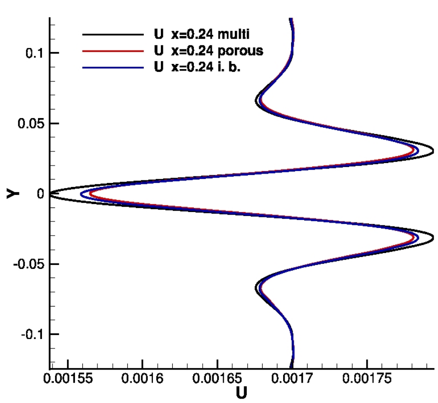


(a) $x = 0.24m$

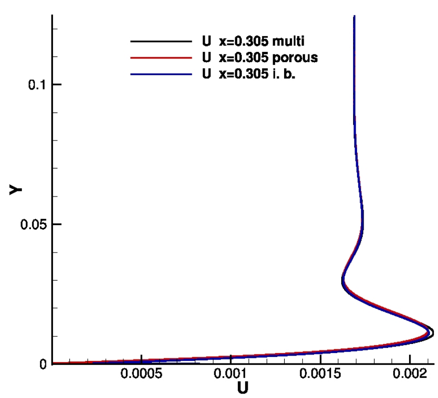


(b) $x = 0.305m$

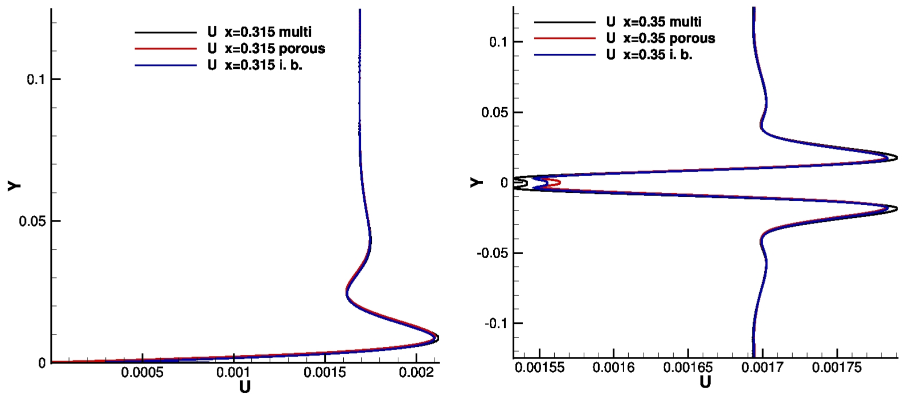


(c) $x = 0.315m$ (d) $x = 0.35m$

FIG. 6.4. *Vertical profiles of the $u_1$–velocity component in the different distances.*

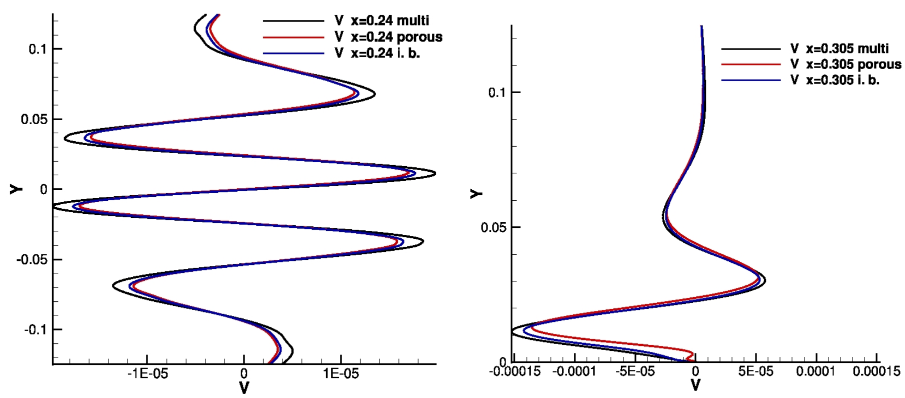


(a) $x = 0.24m$ (b) $x = 0.305m$

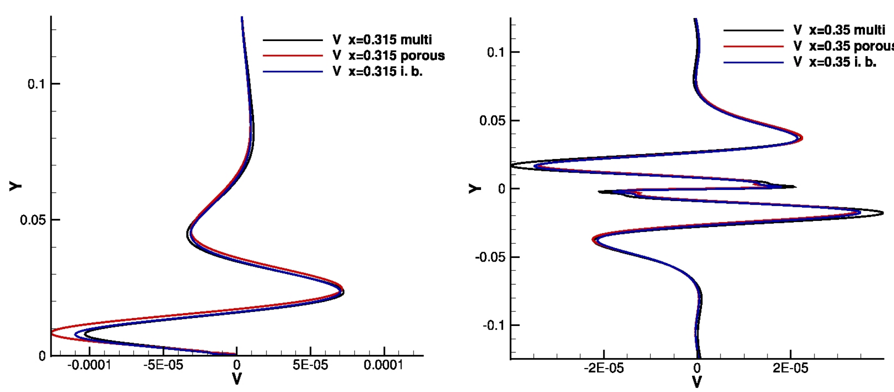


(c) $x = 0.315m$ (d) $x = 0.35m$

FIG. 6.5. *Vertical profiles of the $u_2$–velocity component in the different distances.*

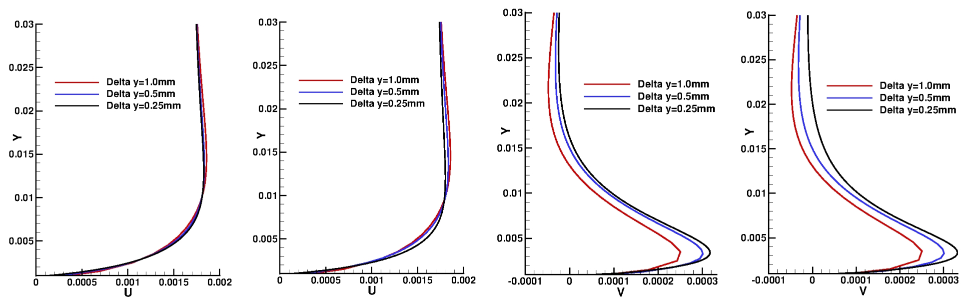


(a) porous (b) immersed b. (c) porous (d) immersed b.

Fig. 6.6. *Vertical profiles of the $u_1$ (left) and $u_2$ (right) velocity components in the point $x = 0.305m$ for porous and immersed boundary approach.*


[4] Baines P.: Topographic effects in stratified flows. Cambridge University Press, 1997.

[5] Fernando H., Hunt J.: Turbulence, waves and mixing at shear free density interfaces. Part 1. Theoretical model. *J. Fluid Mech.* **347**, 197–234, 1997.

[6] Meunier P., Spedding G.: Stratified propelled wakes. *J. of Fluid Mech.* **552**, 229–256, 2006.

[7] Hanazaki H., Kashimoto K., Okamura T.: Jets generated by a sphere moving vertically in a stratified fluid. *J. of Fluid Mech.* **638**, 173–197, 2009

[8] Sutherland B., Linden P.: Internal wave excitation from stratified flow over a thin barrier. *J. Fluid. Mech.* **377**, 223-252, 1998.

[9] Castro I.: Weakly stratified laminar flow past normal flat plates. *J. Fluid Mech.* **454**, 21-46, 2002.

[10] T. Bodnár, L. Beneš, Ph. Fraunié, K. Kozel Application of compact finite-difference schemes to simulations of stably stratified fluid flows. Applied Mathematics and Computation **doi:10.1016/j.amc.2011.08.058** Article in press.

[11] Dick E., Vierendeels J., Riemslagh K.: A multigrid semi–implicit line–method for viscous incompressible and low–mach–number flows on high aspects ratio grids. Journal of Computational Physics **154** 310–341 (1999)

[12] Beneš L., Fürst J., Fraunié Ph.: Numerical simulation of the towing tank problem using high order schemes. BAIL 2008 - Boundary and Interior Layers. Lecture Notes in Computational Science and Engineering 69, Springer 2009 ISSN 1439-7358.

[13] Beneš L., Fürst J.: Numerical simulation of the Stratified Flow Past a Body. *Numerical Mathematics and Advanced Applications. ENUMATH 2009.* Berlin: Springer, 2010, p. 155-162. ISBN 978-3-642-11794-7.

[14] Beneš L., Fürst J., Fraunié Ph.: Numerical simulation of the stratified flow using high order schemes. *E*ngineering Mechanics, 16(1):39–48, 2009. ISSN 1210-2717.

[15] Beneš L., Fürst J., Fraunié Ph.: Comparison of two numerical methods for the stratified flow. *J.* Computers & Fluids,in press, doi:10.1016/j.compfluid.2011.02.003.

[16] Chaschechkin Y.D., Mitkin V.V.: Experimental study of a fine structure of 2D wakes and mixing past an obstacle in a continuously stratified fluid. *Dyn. Atmos. Oceans* 34, 165–187, 2001

[17] Mittal R., Iaccarino G.: Immersed Boundary Methods. *Annu. Rev. Fluid Mech.***37**, 239–261.

[18] Fadlun A.A., Verzicco R., Orlandi P., Mohd–Yusof J.: Combined Immersed–Boundary Finite–Difference Methods for Three–Dimensional Complex Flow Simulations. *J. Comp. Phys.*, **161**(2000), 35–60.

[19] Berrabaa S., Fraunié Ph., Crochet M.: 2D Large Eddy Simulation of Highly Stratified Flow: The Stepwise Structure Effect. *Advances in Computation: Theory and Practise*, **7**, 179–186.

[20] Hemker P.W., Koren B.: Multigrid, defect correction and upwind schemes for the steady Navier-Stokes equations. Numerical methods for fluid dynamics III; *Clarendon Press/Oxford University Press*, 1988, p. 153-170.

[21] Janowitz GS.: The slow transverse motion of a flat plate through a non-diffusive stratified fluid. In:*J. Fluid Mech.* **47. 1**,p.171-181. 1971.

[22] E. Arquis and J.P. Caltagirone: Sur les conditions hydrodynamiques au voisinage d'une interface milieu fluide - milieu poreux: application a la convection naturelle. C.R. Acad. Sci. Paris II 299 (1984), pp. 1–4.

[23] Bodnár T., Beneš L.,Kozel K.: Numerical simulation of flow over barriers in complex terrain, *Il Nuovo Cimento*, **31 C,** N. 5-6, p.619-632, 2008.